Available online at www.sciencedirect.com
ScienceDirect
Journal of Catalysis 243 (2006) 192–198
JOURNAL OF CATALYSIS
www.elsevier.com/locate/jcat

Theoretical study of H_2O dissociation and CO oxidation on $Pt_2Mo(111)$

J.G. Wang, B. Hammer *

Interdisciplinary Nanoscience Center (iNANO) and Department of Physics and Astronomy, University of Aarhus, DK-8000 Aarhus C, Denmark

Received 7 April 2006; revised 30 June 2006; accepted 6 July 2006

Abstract

We investigate by means of density functional theory the adsorption and catalytic oxidation of CO by H_2O on a fully water-covered $Pt_2Mo(111)$ surface. We model the presence of water on the surface by a double water bilayer. The calculations aim to quantify the role of the proposed mechanisms underlying the CO-tolerant behavior of Pt-based anode materials for low-temperature fuel cells. We found that the Pt_2Mo surface is more CO-tolerant than the pure Pt surface, for two reasons. The *ligand effect*, in which the CO coverage is lowered through a reduced binding energy at the Pt sites of the alloyed surface, is supported by calculated CO binding energies of 0.3–0.4 eV on the water-covered alloy surface versus much higher binding energies (0.8–1.2 eV) on the water-covered Pt surface. The *bifunctional mechanism*, in which H_2O dissociates into OH, which in turn oxidizes adsorbed CO into CO_2, is also evident from our calculations. Although the dissociation of water on Pt(111) is a highly endothermic reaction ($\Delta E \sim 0.5$–0.6 eV), it becomes almost a thermoneutral reaction on $Pt_2Mo(111)$, because the Mo sites bind the OH groups more strongly. The oxidation of the adsorbed CO is calculated to proceed via formation of an adsorbed COOH intermediate. Depending on the initial CO adsorption site, we calculate the COOH formation energy to be as low as 0.18 eV meaning that CO oxidation should become possible at moderate overpotentials. In terms of the H_2O dissociation step, the $Pt_2Mo(111)$ alloy surface is superior to similar PtNi and PtRu alloy surfaces.

Keywords: PEM fuel cells; Anode materials; CO tolerance; Water splitting; CO oxidation; Bifunctional mechanism; Density functional theory; Pt; PtMo; PtRu; PtNi

1. Introduction

The development of CO-tolerant anode materials for low-temperature fuel cells is desirable, because using such materials imposes less constraints to the purification of the H_2 feedstock and opens the possibility of using, for example, online reformed methanol [1–4]. A practical strategy toward making CO-tolerant anode materials is to slightly modify anodes based on pure metallic platinum that suffers from CO poisoning but is otherwise an excellent electro-oxidation catalyst. This modification may be done by adding a second metallic component, including Ru [5–7], Mo [8–16], Sn [17–20], and Fe, Co, Ni [21–23]. At present, PtRu or PtSn alloys are widely used anode materials for commercial fuel cell applications. Recently, several experimental [8–16] and theoretical [24] studies have revealed that PtMo alloys exhibit better CO tolerance than PtRu alloys. An advantage of Mo as a potential CO-tolerant anode electrocatalyst is its high abundance and low cost compared with the limited availability and high price of Ru [15,25]. Two lines of reasoning have been proposed to explain the improved CO tolerance caused by the addition of a second metal (Ru, Mo, and Sn) to Pt. One of these involves a *bifunctional mechanism* of the surface [26], and the another focuses on a *ligand effect* (or electronic effect) [27,28]. In the bifunctional mechanism, the surface catalyzes simultaneously the dissociative adsorption of water into OH on the surface sites of the second metal and the oxidation reaction between this OH and CO adsorbed on the Pt sites. The CO is thus removed as CO_2. When invoking the ligand effect, the CO tolerance is explained by the second metal changing the electronic structure of the Pt such that the CO adsorption energy becomes reduced. The electronic effect [24,29,30] has been rationalized in terms of the Hammer–Nørskov d-band model [31,32], which states that on changing the chemical and structural composition of a late transition metal surface, the main effect on adsorbate binding energies can often be traced to an energetic shift of the

* Corresponding author.
E-mail address: hammer@phys.au.dk (B. Hammer).
URL: http://www.phys.au.dk/~hammer/.

0021-9517/$ – see front matter
doi:10.1016/j.jcat.2006.07.009

metal valence *d*-states. There is no general consensus on the role of Mo in causing improved CO tolerance. Some studies conclude that the bifunctional mechanism is active [14,16] whereas others emphasize the role of Mo additives in significantly modifying the CO adsorption/desorption characteristics on Pt, leading to lower CO desorption temperatures compared with monometallic Pt/TiO_2 catalysts [15]. A recent study by Mylswamy et al. [13] found that the *d*-orbital vacancy increased with increasing Ru or Mo content, pointing in the direction of the ligand effect. There are numerous theoretical studies on water dissociation and CO oxidation on Pt and PtRu systems [24,28,29,33–37]. However, we chose to study a PtMo alloy system because of the recent experimental interest in this system. In a preceding study, we analyzed the structure and energetics of CO adsorption and water dissociation on pure Pt(111) covered by a double water bilayer [38]. CO adsorption was found to be highly favorable with binding energies in the 0.8–1.2 eV range depending on adsorption site. Water dissociation, on the other hand, was hindered by a high reaction energy (0.5–0.6 eV). In the present work, we alloyed the Pt with Mo and found that the CO adsorption energy was greatly reduced on the Pt surface sites and the water dissociation on the Mo surface sites became almost thermoneutral (0.03–0.10 eV). Substituting the Mo with Ni or Ru, a lesser effect on the water dissociation was calculated. For the $Pt_2Mo(111)$ surface, we also investigated the full CO oxidation by the OH and found favorable reaction energetics, with the COOH reaction intermediate only 0.18 eV less stable than adsorbed CO and OH. We present evidence that both the ligand effect and the bifunctional mechanism are causing the improved CO tolerance of PtMo anode materials.

2. Method

The first-principles density functional theory (DFT) calculations were performed using the DACAPO package [39–41] with a plane-wave basis set ($E_{cut} = 25$ Ry) [42] and ultrasoft pseudopotentials [43]. The generalized gradient approximation (GGA) with the revised Perdew–Burke–Ernzerhof (RPBE) functional [39] was used to describe the exchange-correlation (XC) effects. An electronic temperature of 0.1 eV was used for assigning occupation numbers to one-electron states [44]. A (3×3) $Pt_2Mo(111)$ surface unit cell was used together with a 2×2 *k*-point sampling grid. In a previous study [38], we showed that five or six Pt layers were needed to converge the water dissociation energy (in a double water bilayer) to a level below 0.05 eV. Consequently, here we used a six-layer slab. It is known from experiments that PtMo alloy systems form solid solutions with very weak Pt segregation to the surface [45]. Neglecting the segregation, in the present work the slab was composed of six layers, each with a Pt:Mo ratio of 2:1 and a random distribution of the Pt and Mo atoms. A calculated bulk Pt_2Mo lattice parameter of 4.00 Å was used. For the Pt_2Ni and Pt_2Ru slabs, the calculated lattice constants were 3.95 and 3.96 Å. On one side of the slab was a double water bilayer with 12 water molecules per surface (3×3) cell in the most stable H-up configuration determined on Pt(111) [38]. The water system is essentially a thin ice-Ih film. During the optimization process, the topmost alloy layer, all molecules and solvated protons in the water film, and all adsorbed molecules (CO, OH, and H) were relaxed while the remaining alloy layers were kept fixed. The geometries were considered converged when the total residual force is <0.05 eV/Å. Transition states (TSs) were searched using the nudged elastic band (NEB) method [46].

3. Results and discussion

3.1. CO adsorption

The structure of the double water bilayer on $Pt_2Mo(111)$ is shown in Fig. 1a. Each water bilayer sets up a honeycomb pattern with the oxygen atoms centered over atop sites in the surface. This leaves some vacant atop sites where CO may adsorb without disrupting the water structure. For such a *vacant atop* Pt site adsorption configuration, Fig. 1b, the CO adsorption potential energy is −0.29 eV (meaning that the CO binding energy is 0.29 eV), much lower than the calculated adsorption potential energy of −0.77 eV at the corresponding site on the double water bilayer-covered Pt(111) surface [38]. Similar behavior is found when the CO is adsorbed substitutionally at a Pt atop site where a water molecule must be removed, Fig. 1c. Table 1 gives the precise adsorption potential energies that show a ∼0.5-eV destabilization of the CO adsorption at the water-substitutional Pt site. The potential energy for water-substitutional adsorption is evaluated under the assumption that the water readsorbs elsewhere in an ice-like environment, meaning that the calculated sublimation energy of ice is involved in the calculation, as described previously [38]. For completeness, we also consider in Table 1 adsorption of CO that substitutes a water molecule at a Mo site. This CO adsorption energy is seen to be comparable, but slightly smaller (numerically) than the CO adsorption energy at water-substitutional Pt sites, meaning that an ensemble of Pt and Mo sites will be CO-covered. In this context, it is instructive to consider the CO adsorption at metal and alloy slabs in the absence of the double water bilayer. Restricting

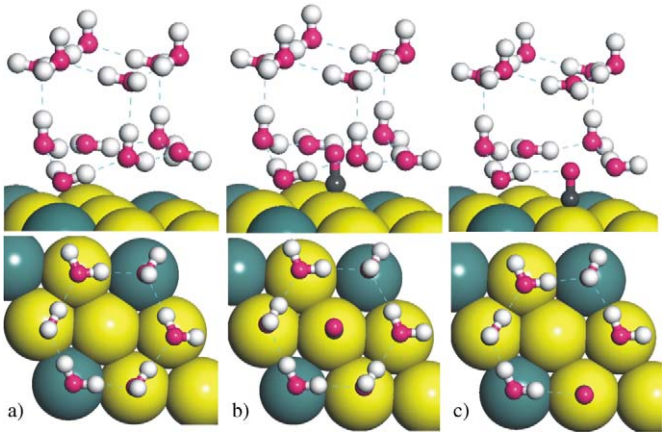

Fig. 1. Structure of the double water bilayer (a) without adsorption of CO, (b) with CO adsorbed at the vacant Pt atop site, (c) with CO adsorbed substitutionally at a water site. In the top views, the topmost water bilayer is omitted for clarity.

Table 1
CO adsorption potential energies (in eV) and double water bilayer formation energies (in eV/H_2O) on Pt_2Mo(111) and Pt(111) (in parenthesis). In the absence of CO, the double water bilayer formation energies are averaged over the 12 H_2O molecules in the calculational cell. In the presence of CO, the formation energies are averaged over the 11 H_2O molecules in the calculational cell and the reference system is the Pt_2Mo (Pt) surface with the CO relaxed in the same atop position as in the presence of the double water bilayer. When CO substitutes H_2O at a Mo site, the Mo site with a low-lying H_2O is chosen (lower left Mo atom in Fig. 1a)

		CO Pt_2Mo(Pt)	H_2O Pt_2Mo(Pt)
No CO	Fig. 1a		−0.558 (−0.518)
CO at vacant Pt	Fig. 1b	−0.29 (−0.77)	−0.498 (−0.475)
CO substitutional H_2O at Pt	Fig. 1c	−0.42 (−1.00)	−0.491 (−0.475)
CO substitutional H_2O at Mo		−0.31 (−1.17)	−0.450 (−0.491)

the CO adsorption site to the Pt atop site, we find CO adsorption potential energies of −1.28 and −1.02 eV on the Pt(111) and Pt_2Mo(111) surfaces, respectively. On the atop Mo site of the Pt_2Mo(111), the corresponding CO adsorption potential energy becomes −1.36 eV, which signifies stronger bonding on Mo than on Pt, as would be expected. The somewhat counterintuitive result that in the presence of the double water bilayer, the substitutional CO adsorption is stronger on the Pt site than on the Mo site can be explained by the fact that the 11 H_2O molecules in the calculational cell are destabilized by 0.45 eV (11 times the difference between −0.491 and −0.450 eV, see Table 1) on substitution of a water molecule over Mo rather than over Pt. This in turn demonstrates that a surface Mo site contributes more favorably to the binding of the double water bilayer than a surface Pt site, meaning that despite the stronger CO binding on Pt sites of the alloy, the double water bilayer provides a driving force for the presence of Mo in the surface layer of the alloy. Consequently, in what follows we maintain a 2:1 ratio of Pt to Mo sites in the alloy surface and focus on the chemistry of the slightly favored CO molecules at Pt sites. The distance between Pt and the carbon atom of CO increases ever so slightly (1.849 vs 1.870 and 1.840 vs 1.858 Å for Figs. 1b and 1c) from Pt(111) to Pt_2Mo(111) substrates. This suggests that the decreased CO bonding on alloying Pt with Mo is attributable to electronic effects rather than structural effects. Referring again to the −1.28 and −1.02 eV adsorption potential energies of CO on Pt atop sites in Pt(111) and Pt_2Mo(111) in the absence of water, we note that the ∼0.25 eV decrease in CO adsorption bond strength on alloying with Mo coincides with a shift in the Pt *d*-band center from −2.43 to −2.79 after the addition of Mo, indicating that much of the reduced CO binding on Pt sites can be considered a consequence of ligand or electronic effects, according to the predictions of the Hammer–Nørskov *d*-band model [31,32]. We note that one experiment has shown direct evidence of CO–Pt bond weakening caused by Mo, although the interpretation is more involved [15].

3.2. H_2O dissociation

Considering the changes in the structure of the double water bilayer on alloying the Pt(111) with Mo provides some information on the role of the Mo. Most prominent is the change in the position of the water molecule that coordinates to a Mo site in the surface. In the absence of CO, Fig. 1a, it obtains an O–Mo bond length of 2.43 Å, considerably smaller than the O–Pt bond length of 2.95 Å for the same water molecule before alloying with Mo. In the presence of CO, the corresponding changes are from 3.01 to 2.53 and from 3.09 to 2.61 Å for the situations depicted in Figs. 1b and 1c. The considerably smaller bond lengths with Mo are accompanied by an increase in the average H_2O bond strength in the double water bilayer over the alloy surface of 40 meV/H_2O without CO and 16–23 meV/H_2O with CO at the vacant site or substituting a Pt-bound H_2O, see Table 1. Because we have 11 or 12 H_2O molecules in the calculational cell, this translates into about 0.2–0.5 eV further bonding of the double water bilayer to the Pt_2Mo(111) surface relative to the Pt(111) surface. As discussed above, substituting the water bound to the Mo site with CO leads to a 41 meV/H_2O destabilization of the water layer (0.45 eV per cell), again indicating strong water-Mo binding. We now consider the first step in the bifunctional mechanism: dissociation of H_2O in the double water bilayer. Two kinds of dissociation pathways are investigated in this study: heterolytic and homolytic. The heterolytic dissociation pathway results in the formation of an adsorbed OH intermediate, OH_a; an ionized hydrogen atom in solution, $H_s^{\delta+}$; and some compensating electronic charge in the slab, δe^-, where δ is expected to be close to 1:

$$H_2O \longrightarrow OH_a + \delta e^- + H_s^{\delta+}, \quad \delta \simeq 1.$$

In contrast, the homolytic dissociation pathway results in the formation of a hydroxyl intermediate and a hydrogen adsorbed on the Pt_2Mo(111):

$$H_2O \longrightarrow OH_a + H_a.$$

In our previous study, we investigated numerous different pathways for each of the two types of dissociation modes (heterolytic and homolytic) [38]. From this, we identified the energetically most favorable heterolytic and homolytic dissociation pathways over Pt(111). In this study, we have adapted these pathways for the Pt_2Mo(111) system choosing in every case the OH_a to form over the Mo site, because this was the site with the shortest H_2O-surface separation. Because assumptions are made for the reaction sites and pathways, the reported activation energies are upper bounds. As shall become apparent, the activation energies found are generally much smaller than for the Pt(111) surface; consequently, we can safely conclude that the Pt_2Mo(111) is more reactive than Pt(111) despite omitting a new search for the most favorable reaction pathways. The final states after dissociation of a water molecule in the double water bilayer are shown in Fig. 2. Without CO or with CO in the vacant atop site, the heterolytic pathway, Figs. 2a and 2b, involves the dissociation of a low-lying H_2O on the Mo site and the dislocation of a proton on an adjacent water molecule. The net result is the creation of an adsorbed OH and a hydronium ion, H_3O^+, at next-nearest neighbor sites. With CO in a water-substitutional site, the heterolytic pathway, Fig. 2c, simply becomes the transfer of a hydrogen atom from the H_2O

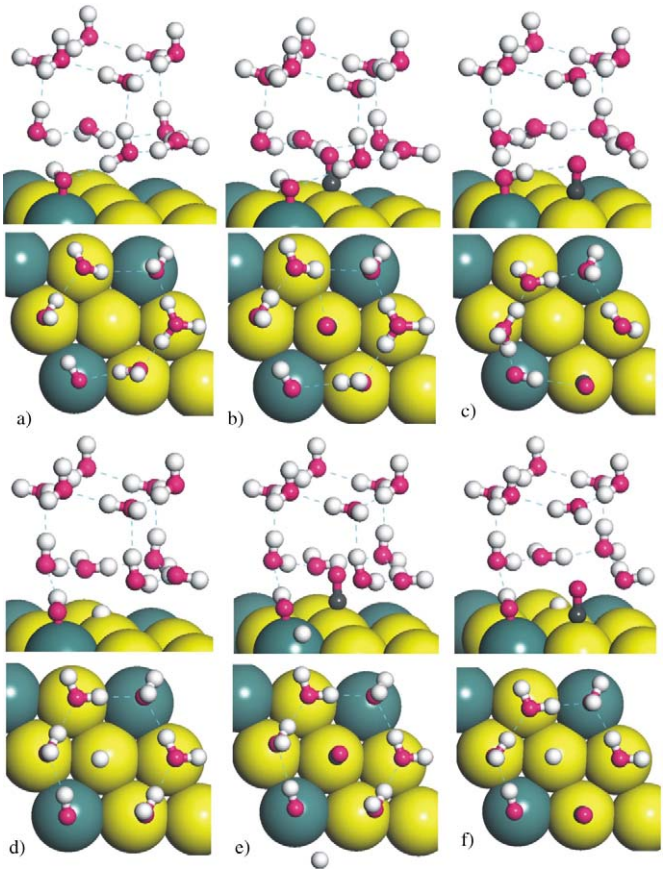

Fig. 2. Side and top views of the final states after water dissociation in a double water bilayer on $Pt_2Mo(111)$. Heterolytic pathways: (a) in absence of CO, (b) with CO adsorbed over a vacant Pt atop site, (c) with CO substituting an H_2O. Homolytic pathways: (d) in absence of CO, (e) with CO adsorbed over a vacant Pt atop site, (f) CO substituting an H_2O.

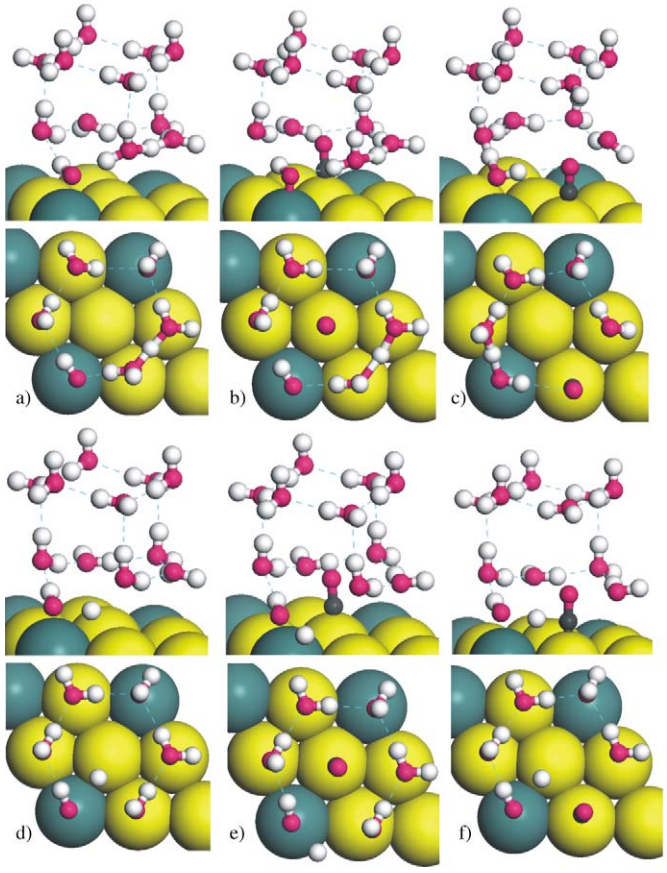

Fig. 3. Side and top views of the transition states during water dissociation in a double water bilayer on $Pt_2Mo(111)$. Subfigures are organized as in Fig. 2: (a)–(c) heterolytic pathways, (d)–(f) homolytic pathways.

on the Mo site to a neighboring H_2O. For the homolytic dissociation pathway, Figs. 2d–2f, the H_2O over the Mo site is dissociated and the hydrogen atom is readsorbed over Pt or Mo top sites in accordance with our findings for Pt(111) [38]. The calculated transition states for the water dissociation reactions are shown in Fig. 3. The transition states along the heterolytic pathways, Figs. 3a–3c, are characterized by extended O–H–O distances for the dislocating protons and by shortened distances between Mo and the oxygen of the dissociating H_2O. The transition states for the homolytic pathways, Figs. 3d–3f, involve H located in surface bridge sites. The reaction and activation energies for the dissociation of H_2O in the double water bilayer on $Pt_2Mo(111)$ are reported in Table 2, where the values for Pt(111) are included in parentheses for comparison [38]. For every combination of initial state and reaction pathway considered, the energetics of water dissociation are higher over $Pt_2Mo(111)$ than over Pt(111). The most favorable situations occur for water dissociation in the presence of CO, where the reaction energies are 0.03–0.14 eV for heterolytic pathways and 0.10–0.29 eV for homolytic ones. The smaller reaction energies for water dissociation on the alloy surface may be attributed in part to the calculated lower work function over $Pt_2Mo(111)$ ($W = 5.02$ eV) compared with that over Pt(111) ($W = 5.56$ eV), which will favor the electronegative reaction

Table 2
Reaction energy, ΔE, and activation energy, E_a (in eV), for H_2O dissociating in the double water bilayer over $Pt_2Mo(111)$ and (in parenthesis) over Pt(111)

	Heterolytic pathways		Homolytic pathways	
	ΔE	E_a	ΔE	E_a
No CO	0.37 (0.60)	0.52 (0.99)	0.40 (0.71)	0.90 (1.35)
CO at vacant site	0.14 (0.52)	0.46 (0.95)	0.29 (0.74)	0.78 (1.15)
CO substituting water	0.03 (0.52)	0.10 (0.53)	0.10 (1.14)	0.75 (1.37)

product, adsorbed OH [47]. The activation energies are very large for the homolytic pathways, indicating that our calculations predict heterolytic pathways (transfer of the dissociating hydrogen to the water network) as the dominant reaction mechanism at a water/$Pt_2Mo(111)$ interface, as was previously found for a water/Pt(111) interface in previous studies [38,48]. We further investigated the dissociation of water in a double water bilayer on two other promising Pt-alloys, Pt_2Ni and Pt_2Ru. The dissociation energies of H_2O on these Pt alloy systems are shown in Fig. 4. Whether or not CO is co-adsorbed, a trend is clear: The dissociation energy of H_2O decreases in the order of Pt, Pt_2Ni, Pt_2Ru, Pt_2Mo. This follows the trend in the dissociative O_2 binding energies to Pt, Ni, Ru, and Mo surfaces, which are reported as −2.17, −3.90, −4.62, and −7.48 eV at low-coordinated metal sites [49]. This is strongly suggestive of the oxidation potential of the respective alloy constituents be-

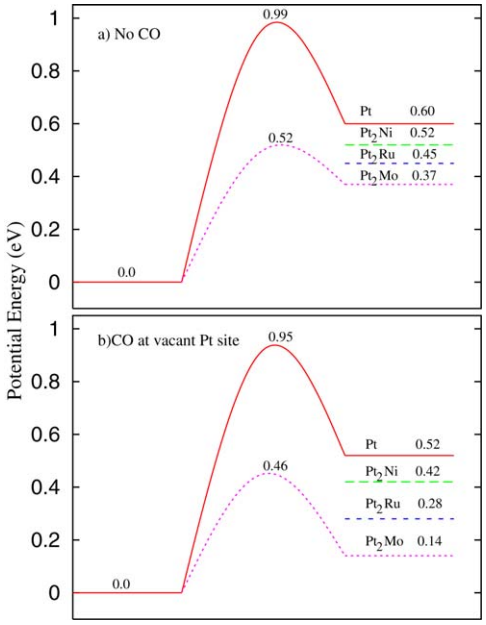

Fig. 4. Potential energy diagram for H_2O dissociation in the double water bilayer on a series of Pt alloys (a) without CO and (b) with CO adsorbed at the vacant Pt atop site.

ing responsible for its ability to catalyze the water dissociation [50,51].

3.3. CO oxidation

Once an adsorbed OH has resulted from the dissociation of H_2O, the second step in the bifunctional mechanism—oxidation of some adsorbed CO by the OH—becomes relevant. In Section 3.2, we argued that the OH forms at the atop Mo site. This is now the starting point for the CO oxidation, and we chose to investigate CO initially adsorbed in the vacant atop site, Fig. 5a, or in the water-substituting site atop Pt, Fig. 5d. Whether the OH formation proceeded via the homolytic or heterolytic pathway will be neglected by omitting the H (either adsorbed on the surface or dissolved in the double water bilayer) while keeping the supercell charge-neutral. The rational for omitting the H is that in an operating fuel cell, it will split in to a proton and an electron that then migrate to the cathode side of the cell, where they recombine and react with O_2 to form water [52,53]. The excess energy of this reaction less the overpotential set up by the endothermicity of the water dissociation on the anode will allow the electron to perform work on its way to the cathode. We find that CO oxidation by OH proceeds via formation of an adsorbed reaction intermediate, COOH. The calculated structure of the intermediate is shown in Fig. 5, together with the transition states for its formation and its decomposition into CO_2 and a proton in solution. In forming the COOH, the adsorbed CO and OH dislocate slightly from the atop sites. In the transition state, the CO–OH distance is 1.82 and 1.86 Å, depending on whether CO in the vacant atop site (Fig. 5a) or water-substituting CO (Fig. 5d) is considered. Once formed, the CO–OH bond distance becomes 1.44 and 1.47 Å in the two cases (Figs. 5b and 5e, respectively).

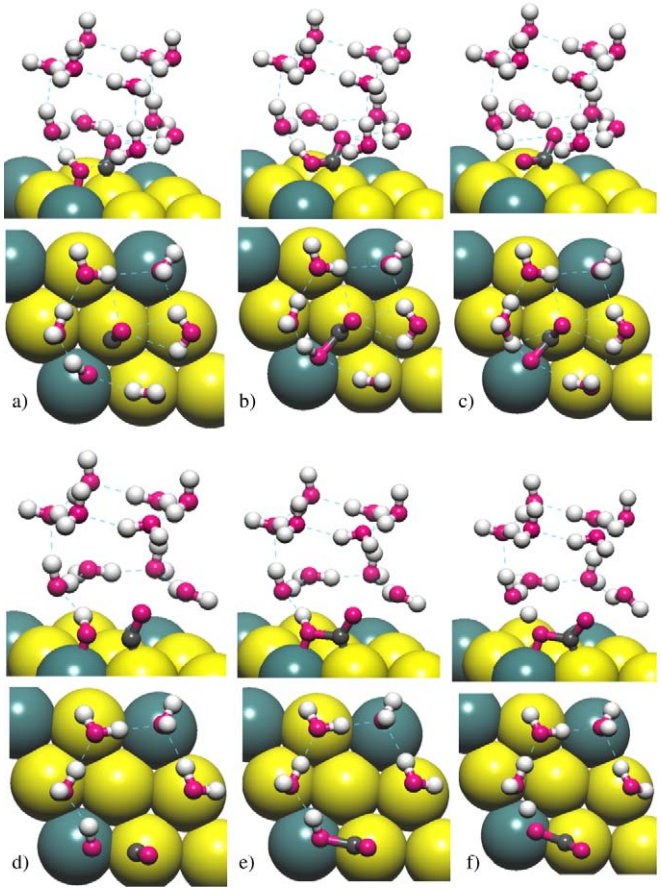

Fig. 5. Side and top views of the transition state for COOH formation, the intermediate state of COOH, and the transition state for $CO_2 + H$ formation in a double water bilayer on $Pt_2Mo(111)$. (a)–(c) With CO adsorbed over a vacant Pt atop site, (d)–(f) with CO substituting a H_2O at a Pt site.

The hydrogen bonds between the COOH and the water network have initial lengths of 2.13 and 1.71 Å for CO at the vacant atop site (Fig. 5b) and 1.99 Å for CO substituting a water molecule (Fig. 5e). The reaction energy for COOH formation is calculated to be only a few tenths of an eV, and the activation energy is well below 0.5 eV. The precise numbers that depend on the initial position of the CO are given in Fig. 6. The dissociation of the COOH is now the final step in forming CO_2. Given that the heterolytic pathways were most favorable for water dissociation, we assume that the COOH dissociation proceeds via a heterolytic pathway as well. The transition state structures for the COOH dissociation reaction step are shown in Figs. 5c and 5f for CO initially at the vacant atop site and substituting water, respectively. The HO–CO bond is now only 1.39 and 1.42 Å, the dissociating COO–H bond is 1.38 and 1.28 Å, and the H_2O–HOOC separation is 1.26 and 1.36 Å in the two transition states, respectively. From the energetics of the COOH dissociation also included in Fig. 6, it is seen that this reaction step is particularly facile. With activation energies of only 0.07 and 0.11 eV (for CO initially either at the vacant atop site or substituting a water molecule), this reaction step will be very fast at any reasonable temperature, meaning that the COOH is only a transient intermediate. We note that a backward reaction in which the COOH decomposes again into adsorbed CO and

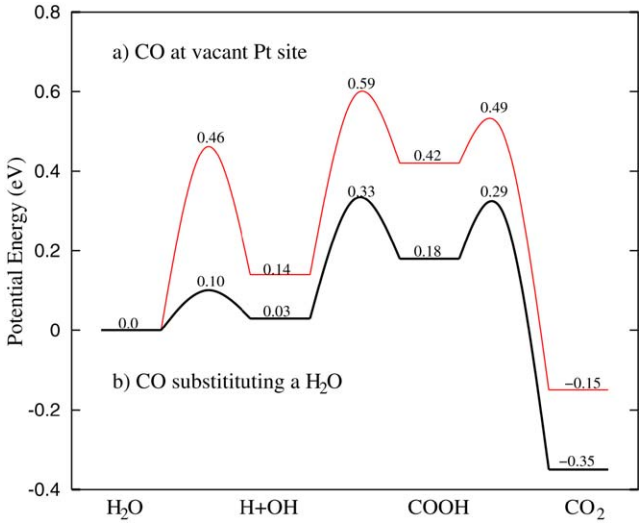

Fig. 6. Potential energy diagram for heterolytic H_2O dissociation and CO oxidation in a double water bilayer on $Pt_2Mo(111)$ with (a) CO adsorbed on a vacant Pt atop site or (b) with CO substituting a H_2O at a Pt site.

OH is subject to slightly larger barriers (0.11 and 0.15 eV) for the two initial CO positions, further supporting the forward reaction and the eventual formation of CO_2. The overall reaction energy is such that 0.15–0.35 eV is gained at the stage where CO_2 is formed and two protons are solvated. Reducing $\frac{1}{2}O_2$ to H_2O with these protons at the cathode side involves a further energy release of 1.45 eV [54]. It is interesting to compare the present calculations of CO oxidation by OH at a water-solid catalyst interface with calculations for a gas–solid catalyst interface. Using a Pt(111) slab model, Shubina et al. [55] found the COOH to form with a barrier of 0.58 eV and a reaction energy of −0.60 eV. In another slab model study of Pt(111), Gong et al. [56] found activation energies of 1.02 and 0.59 for the COOH decomposition reactions forming either $CO_2 + H$ (our forward reaction) or CO + OH (our backward reaction). The much lower activation energies calculated in our work are attributable to the presence of the water environment, which is capable of forming hydrogen bonds to the dissociating COOH and of solvating protons that are transferred. This conclusion confirms the findings of Gong et al. [56] and Desai et al. [48] also showing the important role of hydrogen bonds in connection with CO oxidation in solution. In our case, however, some of the effects are also likely to be related to the Mo alloy component.

4. Conclusion

We have presented DFT calculations of the CO adsorption and oxidation by H_2O on a water-covered $Pt_2Mo(111)$ model anode surface. The CO adsorption bond strength is found to be reduced by about 0.5 eV on the alloy surface compared with on a Pt(111) reference surface. The water dissociation leading to adsorbed OH is on the order of 0.5 eV more favorable on the alloy surface, and the reaction thereby becomes almost thermoneutral. This means that in an electrochemical cell, only a small overpotential is required to form OH on the alloy surface. The further reaction of this OH with adsorbed CO involves only minor reaction energies and moderate activation barriers. A COOH reaction intermediate is formed at an energy cost of 0.15–0.3 eV depending on the initial position of the CO. The COOH complex readily decomposes, releasing CO_2. We thus find two possible reasons why a PtMo alloy may be a superior anode material for low-temperature fuel cell applications with CO contamination of the H_2 feedstock: (i) the reduced CO binding energy at the water-alloy interface decreases the CO coverage for a given CO content in the feed stock, or (ii) the favorable reaction energetics for the CO oxidation by H_2O at the water/alloy interface allows for CO oxidation and hence CO removal at moderate overpotentials. In conclusion, our calculations show evidence that both the ligand effect and the bifunctional mechanism are operative for PtMo anode materials. To determine which of these mechanisms is more important would require building a kinetic model on top of the determined energetics, a task beyond the scope of the present work.

Acknowledgments

The authors acknowledge the support from Danish Research Councils and Dansk Center for Scientific Computing.

References

[1] N.M. Markovic, P.N. Ross, Surf. Sci. Rep. 45 (2002) 121.
[2] V. Mehta, J.S. Cooper, J. Power Sourc. 114 (2003) 32.
[3] J.S. Spendelow, A. Wieckowski, Phys. Chem. Chem. Phys. 6 (2004) 5094.
[4] J. Greeley, M. Mavrikakis, Catal. Today 111 (2006) 52.
[5] U.A. Paulus, U. Endruschat, G.J. Feldmeyer, T.J. Schmidt, H. Bonnemann, R.J. Behm, J. Catal. 195 (2000) 383.
[6] T. Kawaguchi, W. Sugimoto, Y. Murakami, Y. Takasu, J. Catal. 229 (2005) 176.
[7] Z. Jusys, J. Kaiser, R.J. Behm, Electrochim. Acta 47 (2002) 3693.
[8] S. Mukerjee, R.C. Urian, S.J. Lee, E.A. Ticianelli, J. McBreen, J. Electrochem. Soc. 151 (2004) A1094.
[9] S. Mukerjee, S.J. Lee, E.A. Ticianelli, et al., Electrochem. Solid State Lett. 2 (1999) 12.
[10] M.R. Tarasevich, V.A. Bogdanovskaya, B.M. Grafov, N.M. Zagudaeva, K.V. Rybalka, A.V. Kapustin, Y.A. Kolbanovskii, Russ. J. Electrochem. 41 (2005) 746.
[11] E.I. Santiago, M.S. Batista, E.M. Assaf, E.A. Ticianelli, J. Electrochem. Soc. 151 (2004) A944.
[12] S. Mukerjee, R.C. Urian, Electrochim. Acta 47 (2002) 3219.
[13] S. Mylswamy, C.Y. Wang, R.S. Liu, J.-F. Lee, M.-J. Tang, J.-J. Lee, B.-J. Weng, Chem. Phys. Lett. 412 (2005) 444.
[14] B.N. Grgur, N.M. Markovic, P.N. Ross, J. Electrochem. Soc. 146 (1999) 1613.
[15] S. Zafeiratos, G. Papakonstantinou, M.M. Jacksic, S.G. Neophytides, J. Catal. 232 (2005) 127.
[16] E.I. Santiago, G.A. Camara, E.A. Ticianelli, Electrochim. Acta 48 (2003) 3527.
[17] V.R. Stamenkovic, M. Arenz, C.A. Lucas, M.E. Gallagher, P.N. Ross, N.M. Markovic, J. Am. Chem. Soc. 125 (2003) 2736.
[18] M.M. Schubert, M.J. Kahlich, G. Feldmeyer, M. Huttner, S. Hackenberg, H.A. Gasteiger, R.J. Behm, Phys. Chem. Chem. Phys. 3 (2001) 1123.
[19] V. Radmilovic, T.J. Richardson, S.J. Chen, P.N. Ross, J. Catal. 232 (2005) 199.
[20] M. Arenz, V. Stamenkovic, B.B. Blizanac, K.J. Mayrhofer, N.M. Markovic, P.N. Ross, J. Catal. 232 (2005) 402.
[21] M. Watanabe, S. Motoo, J. Electroanal. Chem. 206 (1986) 197.
[22] T.C. Deivaraj, W.X. Chen, J.Y. Lee, J. Mater. Chem. 13 (2003) 2555.
[23] A. Sirijaruphan, J.G. Goodman, R.W. Rice, J. Catal. 224 (2004) 304.
[24] T.E. Shubina, M.T.M. Koper, Electrochim. Acta 47 (2002) 3621.

[25] K.C. Kwiatkowski, S.B. Milne, S. Mukerjee, C.M. Lukehart, J. Clust. Sci. 16 (2005) 251.
[26] M. Watanabe, S. Motoo, J. Electroanal. Soc. 60 (1975) 267.
[27] B. Beden, C. Lamy, N.R. De Tacconi, A.J. Arvia, Electrochim. Acta 35 (1990) 691.
[28] E. Christoffersen, P. Liu, A. Ruban, H.L. Skriver, J.K. Nørskov, J. Catal. 199 (2001) 123.
[29] M.T.M. Koper, T.E. Shubina, R.A. van Santen, J. Phys. Chem. B 106 (2002) 686.
[30] P. Liu, J.K. Nørskov, Phys. Chem. Chem. Phys. 3 (2001) 3814.
[31] B. Hammer, Y. Morikawa, J.K. Nørskov, Phys. Rev. Lett. 76 (1996) 2141.
[32] B. Hammer, J.K. Nørskov, Adv. Catal. 45 (2000) 71.
[33] P. Liu, A. Logadottir, J.K. Nørskov, Electrochim. Acta 48 (2003) 3731.
[34] Y. Cai, A.B. Anderson, J. Phys. Chem. B 109 (2005) 7557.
[35] J. Narayanasamy, A.B. Anderson, J. Electroanal. Chem. 554 (2003) 35.
[36] A.B. Anderson, Electrochim. Acta 47 (2002) 3759.
[37] A.B. Anderson, N.M. Neshev, J. Electrochem. Soc. 149 (2002) E383.
[38] J.G. Wang, B. Hammer, J. Chem. Phys. 124 (2006) 184704.
[39] B. Hammer, L.B. Hansen, J.K. Nørskov, Phys. Rev. B 59 (1999) 7413.
[40] S.R. Bahn, K.W. Jacobsen, Comput. Sci. Eng. 4 (2002) 56.
[41] http://www.camp.dtu.dk/campos.
[42] M.C. Payne, M.P. Teter, D.C. Allan, T.A. Arias, J.D. Joannopoulos, Rev. Mod. Phys. 64 (1992) 1045.
[43] D. Vanderbilt, Phys. Rev. B 41 (1990) 7892.
[44] J. Neugebauer, M. Scheffler, Phys. Rev. B 46 (1992) 16,067.
[45] B.N. Grgur, N.M. Markovic, P.N. Ross, J. Phys. Chem. B 102 (1998) 2494.
[46] G. Henkelman, H. Jónsson, J. Chem. Phys. 113 (2000) 9978.
[47] M.T.M. Koper, G.A. Voth, J. Chem. Phys. 109 (1998) 1991.
[48] S. Desai, M. Neurock, Electrochim. Acta 48 (2003) 3759.
[49] T. Bligaard, J.K. Nørskov, S. Dahl, J. Matthiesen, C.H. Christensen, J. Sehested, J. Catal. 224 (2004) 206.
[50] X.-Q. Gong, Z.-P. Liu, R. Raval, P. Hu, J. Am. Chem. Soc. 126 (2004) 8.
[51] X.-Q. Gong, R. Raval, P. Hu, Phys. Rev. Lett. 93 (2004) 106104.
[52] W.B. Kim, T. Voitl, G.J. Rodriguez-Rivera, J.A. Dumesic, Science 305 (2004) 1280.
[53] L. Carrette, K.A. Friedrich, U. Stimming, Fuel Cells 1 (2001) 5.
[54] A.B. Anderson, T.V. Albu, J. Am. Chem. Soc. 121 (1999) 11,855.
[55] T.E. Shubina, C. Hartnig, M.T.M. Koper, Phys. Chem. Chem. Phys. 6 (2004) 4215.
[56] X.-Q. Gong, P. Hu, R. Raval, J. Chem. Phys. 119 (2003) 6324.